Journal of Molecular Liquids 217 (2016) 93–98

Contents lists available at ScienceDirect

Journal of Molecular Liquids

journal homepage: www.elsevier.com/locate/molliq

Theoretical analysis of complex formation of *p*-carboxybenzeneboronic acid with a monosaccharide

Yuki Seno, Norio Yoshida *, Haruyuki Nakano

Department of Chemistry, Graduate School of Science, Kyushu University, 744 Motooka, Nishi-ku, Fukuoka 819-0395, Japan

ARTICLE INFO

Article history:
Received 22 June 2015
Received in revised form 5 December 2015
Accepted 18 December 2015
Available online 18 February 2016

Keywords:
p-Carboxybenzeneboronic acid
Monosaccharide complex
Acid dissociation constant
3D-RISM-SCF

ABSTRACT

Changes in the acid dissociation constant, p*K*a, of *p*-carboxybenzeneboronic acid (PCBA) upon complex formation with monosaccharide are considered by using the three-dimensional reference interaction site model self-consistent field theory. The p*K*a of PCBA is lowered through complex formation, which is consistent with experimental observations. Free energy component analysis of the dissociation reaction was performed to investigate the details of the contribution to the p*K*a shift. The magnitudes of the changes in both the electronic energy and the solvation free energy were smaller for the PCBA-complex than for PCBA. These smaller changes can be attributed to the delocalization of the excess charge and to a reduction of the solvent-accessible area near the boric acid group because of the steric bulk of the monosaccharide.

1. Introduction

The solubility of drug molecules under the physiological conditions in the human body is a crucial issue in pharmacology. Thus, factors that affect the solubility of organic compounds in aqueous medium under physiological conditions have attracted considerable attention in the fields of chemistry and biochemistry as well as in pharmacology. A number of approaches have been used to increase the solubility of compounds under the physiological pH conditions found in the human body [1–3].

One way to increase the solubility of a compound is to change the acidity by combining the drug molecule with another compound. *p*-Carboxybenzeneboronic acid (PCBA), which is considered to be a promising candidate for boron neutron capture therapy (BNCT), is known to have low solubility in aqueous medium under physiological conditions [4–8]. In aqueous solution, at physiological pH, PCBA exists in the equilibrium:

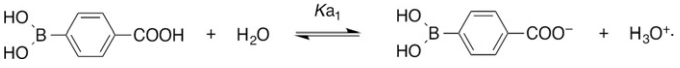

(1)

Under higher pH conditions the following equilibrium forms:

(2)

Here, Ka_1 and Ka_2 denote the dissociation constants of the reactions.

Given that the acid dissociation constant, p*K*a, of reaction (2) is approximately 8.7 (based on ^{11}B NMR measurements), PCBA could not dissociate under physiological conditions at pH 7.4 [9]. This result indicates that PCBA will only be soluble in aqueous solutions that are too alkaline for safe use in the human body [10]. Islam et al. reported that complex formation of PCBA with monosaccharide increases the solubility of the compound at physiological pH [9]. They showed that the complex of PCBA with monosaccharide undergoes a two-step acid dissociation reaction similar to that of PCBA and that the p*K*a values of those reactions are lower for the complex. The change in solubility of PCBA should be closely related to the shift of p*K*a value. However, the origin of the change in solubility is unclear.

In the present study, to determine the origins of the change in solubility at the molecular level, we employed three-dimensional reference interaction site model self-consistent field (3D-RISM-SCF) theory to analyze the acid dissociation reactions of PCBA and of the PCBA-monosaccharide complex in aqueous solution. The 3D-RISM-SCF theory, which is a hybrid of quantum mechanics electronic structure theory and statistical mechanics integral equation theory (IET) of molecular liquids, allows the solvation free energy (SFE) of the solute molecule as well as the solvation structure to be considered at the molecular level [11,12]. This approach has been applied to a range of chemical processes that involve changes in the electronic structure of the solute molecule [13–16]. In addition, the hybrid approaches of the IET and quantum mechanics theory have been successfully applied to evaluate p*K*a [17–20].

In the following sections, we evaluate the reaction free energies, ΔG, of the acid dissociation reactions of PCBA, (1) and (2), and of the PCBA-monosaccharide complex (hereafter, referred to as the

* Corresponding author.
E-mail address: noriwo@chem.kyushu-univ.jp (N. Yoshida).

http://dx.doi.org/10.1016/j.molliq.2015.12.063
0167-7322/

PCBA-complex), which can be directly connected to the acid dissociation constant, p*K*a:

$$\mathrm{p}Ka = -\log Ka = -\log\frac{[A^-][H_3O^+]}{[HA]} = \frac{1}{\ln 10}\frac{\Delta G}{RT}, \quad (3)$$

where HA is a compound that dissociates into A^-, and *R* and *T* denote the gas constant and absolute temperature, respectively. We assume that all the protons exist as hydronium ions, H_3O^+, and that the concentration of water, $[H_2O]$, does not change during the reaction. From the computed p*K*a values, the mole fractions of the three different species (neutral molecule and monovalent and divalent anions) are obtained as a function of pH. The components of the reaction free energy and the solvation structures of PCBA and PCBA-complex are discussed in an attempt to elucidate the origin of the change in solubility upon the complex formation.

2. Computational methods

Density functional theory (DFT) with the B3LYP functional [21] and the 6–31++G(d,p) basis set [22,23] were employed for all the electronic structure calculations performed in this study. Prior to the free energy calculations, the molecular structures of the solute species were optimized by using the polarizable continuum model (PCM). For these optimized structures, the SFEs, the electronic structures of the solute molecule, and the solvent distribution of the PCBA, β-D-galactopyranose, and those of the complex in water at infinite dilution were computed by using the 3D-RISM-SCF theory. Details of the computational conditions are given below.

We employed the Kovalenko–Hirata closure for solving the 3D-RISM equation [11,24,25]. The parameters used in the 3D-RISM-SCF theory were as follows. The temperature was 298 K and the density of solvent water was 1.0 g cm^{-3}. The Lennard-Jones parameters for solute molecules were taken from the general Amber force field (GAFF) parameter set [26,27]. The simple point charge model (SPC/E) parameter set for the geometrical and potential parameters for the solvent water was employed with modified hydrogen parameters ($\sigma = 1.0$ Å and $\varepsilon = 0.046$ kcal mol^{-1}) [28]. The grid points in the 3D-RISM-SCF calculations were 128^3, with a spacing of 0.5 Å.

All of the calculations were performed with a modified version of the GAMESS program package [29], for which the 3D-RISM-SCF theory has been implemented [14,30].

3. Results and discussion

3.1. pKa of PCBA

The acid dissociation reactions (1) and (2) were considered. The reaction free energies and the computed p*K*a values, which are summarized in Table 1, show that there is a rather large discrepancy between the computed p*K*a value of PCBA and the experimental value. This difference stems mainly from the difficulty in evaluating the free energy of a proton. In general, obtaining accurate p*K*a values by using first-principles theory is known to be challenging because of the dependence on the computational methodologies employed, such as the basis functions, density functionals, and solvent models, in addition to the free energy computation of a proton [31]. Several methods have been proposed to circumvent these difficulties. Matsui et al. developed a method to predict the p*K*a by using DFT and the PCM [32]. They showed that the experimental p*K*a values are well reproduced from computed reaction free energy by utilizing the linear correlation relation between them. In line with their method, we have adjusted the computed p*K*a value by a constant shift. We chose several carboxylic acids as reference molecules to determine the p*K*a correction parameter based on the similarity of their molecular structures. The p*K*a values of reference molecules are shown in Table 2 [33–35]. The average of the differences between the computed and experimental values was 16.4; thus, the correction parameter was determined to be $\mathrm{p}Ka_{calib} = 16.4$. The corrected p*K*a values,

$$\mathrm{p}Ka = \mathrm{p}Ka_{comp} - \mathrm{p}Ka_{calib} \quad (4)$$

are summarized in the rightmost column of Table 1. Although the corrected value of $\mathrm{p}Ka_2$ of PCBA (10.6) is still an overestimation of the experimental value (8.7), it is sufficient for our discussion. We use the corrected p*K*a values for the following discussion.

3.2. pKa shift upon complex formation

To consider the effects of complex formation on the solubility of PCBA, the acid dissociation reactions of the PCBA-complex with β-D-galactopyranose were examined. The PCBA-complex is assumed to exist in the following equilibriums in aqueous solution:

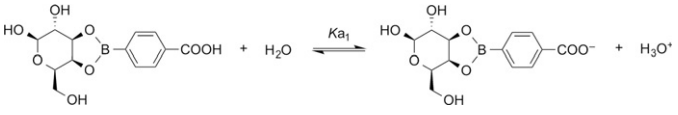

(5)

and

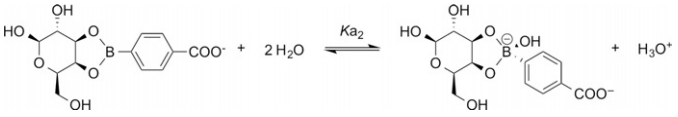

(6)

and we define the acid dissociation constants of the reactions (5) and (6) as $Ka_1 = [HA^-][H_3O^+]/[H_2A]$ and $Ka_2 = [A^{2-}][H_3O^+]/[HA^-]$, respectively. The reaction free energy, the computed p*K*a, and the corrected p*K*a (Table 1) show that complex formation decreases both the first and second p*K*a values. In particular, the second p*K*a changes drastically upon complex formation, which is probably because the reactions (2) and (6) occur at the boric acid group that forms chemical bonds with β-D-galactopyranose.

From the p*K*a values, the distribution of the three chemical species, namely H_2A, HA^-, and A^{2-}, can be obtained as a function of pH: [36]

$$\alpha_0(x) = \frac{[H_2A]}{[H_2A] + [HA^-] + [A^{2-}]} = \frac{1}{1 + 10^x Ka_1 + 10^{2x} Ka_1 Ka_2}, \quad (7)$$

Table 1
Reaction free energies and p*K*a values.

Reaction	Δ*G* [kcal mol^{-1}]	$\mathrm{p}Ka_{comp}$		p*K*a[b]
PCBA + H_2O → $PCBA^-$ + H_3O^+	28.74	21.1		4.7
$PCBA^-$ + $2H_2O$ → $PCBA^{2-}$ + H_3O^+	36.76	26.9	(8.7[a])	10.6
PCBA-complex + H_2O → PCBA-complex$^-$ + H_3O^+	28.13	20.6		4.3
PCBA-complex$^-$ + $2H_2O$ → PCBA-complex^{2-} + H_3O^+	31.22	22.9		6.5

[a] The experimental value taken from Ref. [9].
[b] Adjusted p*K*a values.

Table 2
Comparison of p*Ka* values of the carboxylic acids between the computational, pKa_{comp}, and experimental values, pKa_{explt}. The computational values of the reaction free energy of the acid dissociation reactions, ΔG, and the difference of p*Ka* values, ΔpKa, are also shown.

Molecule	ΔG [kcal mol^{-1}]	pKa_{comp}	pKa_{explt}	ΔpKa
CH_3COOH	28.71	21.0	4.8[a]	16.3
C_4H_9OCOOH	25.92	19.0	3.7[b]	15.3
PhCOOH	29.12	21.4	4.2[c]	17.2
p-F-PhCOOH	28.38	20.8	4.1[a]	16.7
p-Br-PhCOOH	28.08	20.6	4.0[a]	16.6
p-NO_2-PhCOOH	26.52	19.4	3.4[a]	16.0

[a] Ref. [34].
[b] Ref. [35].
[c] Ref. [33].

$$\alpha_{-1}(x) = \frac{[HA^-]}{[H_2A] + [HA^-] + \left[A^{2-}\right]} = \frac{10^x Ka_1}{1 + 10^x Ka_1 + 10^{2x} Ka_1 Ka_2}, \quad (8)$$

$$\alpha_{-2}(x) = \frac{\left[A^{2-}\right]}{[H_2A] + [HA^-] + \left[A^{2-}\right]} = \frac{10^{2x} Ka_1 Ka_2}{1 + 10^x Ka_1 + 10^{2x} Ka_1 Ka_2}, \quad (9)$$

where $\alpha_0(x)$, $\alpha_{-1}(x)$, and $\alpha_{-2}(x)$ denote the mole fractions of neutral, monovalent anion, and divalent anion species H_2A, HA^-, and A^{2-}, respectively, at pH *x*. The mole fractions of H_2A, HA^-, and A^{2-} against pH are plotted in Figs. 1 and 2 for PCBA and the PCBA-complex, respectively. Near the physiological conditions (pH 7.4), PCBA takes the monovalent anion form, whereas the PCBA-complex predominantly takes the divalent anion form, $\alpha_{-2} = 0.89$.

To elucidate the mechanism underlying these changes, the free energy profile of the reaction was decomposed into a number of components. The reaction free energy, ΔG, is expressed as:

$$\Delta G = \Delta E_{solute} + \Delta\delta G_{solv}, \quad (10)$$

where ΔE_{solute} and $\Delta\delta G_{solv}$ denote the change in solute electronic and SFEs, respectively. Note that Δ and δ denote the energy changes due to the reaction and the solvation, respectively. The SFE is further

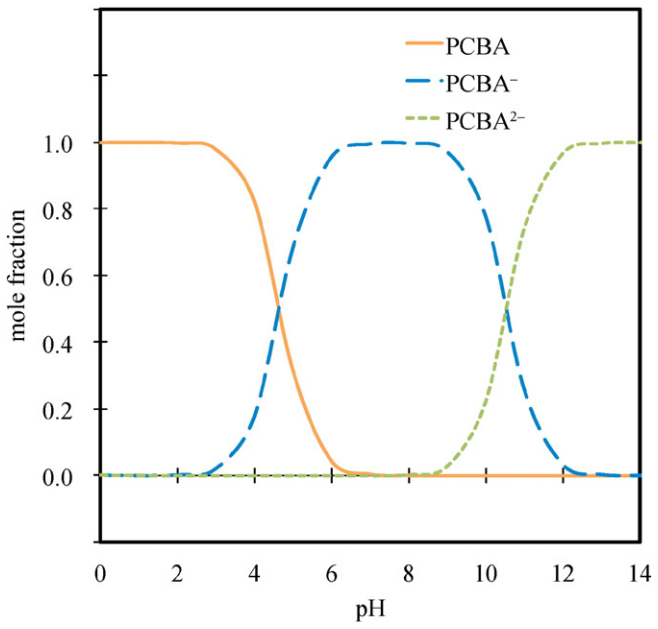

Fig. 1. Distribution of three chemical species of PCBA as a function of pH.

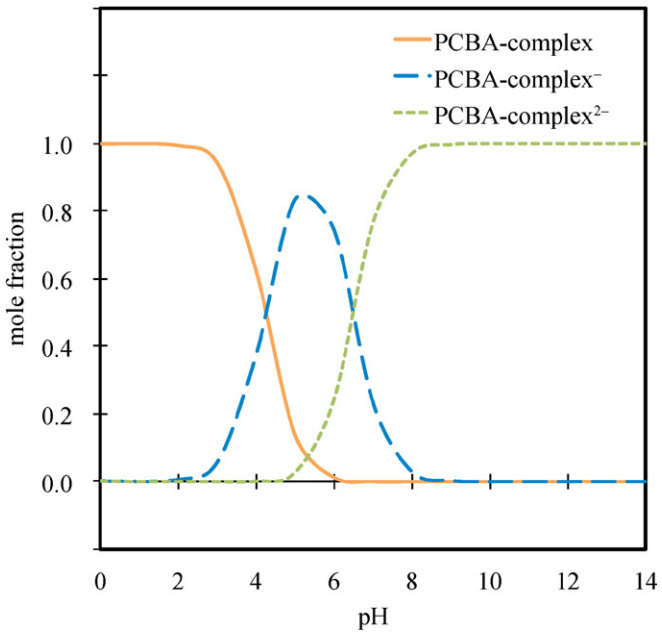

Fig. 2. Distribution of three chemical species of the PCBA-complex as a function of pH.

delineated into the sum of the excess chemical potential, $\delta\mu_{KH}$, and the electronic distortion energy, δE_{dist}:

$$\delta G_{solv} = \delta\mu_{KH} + \delta E_{dist}, \quad (11)$$

where we have employed the Kovalenko–Hirata formula to evaluate the excess chemical potential. The electronic distortion energy means the energy due to the electronic structure change of the solute molecule by solvation.

The components of the reaction free energy of the acid dissociation reactions are summarized in Table 3. The ΔG values of the first acid dissociation reactions for PCBA and the PCBA-complex are similar, namely, 28.74 and 28.13 kcal mol^{-1}, respectively, whereas those of the second acid dissociation reactions show a difference of more than 5 kcal mol^{-1} between PCBA and the PCBA-complex; namely, 36.75 and 31.22 kcal mol^{-1}. In all the reactions, ΔE_{solute} is positive because the excess charge is localized in right hand sides of Eqs. (5) and (6). On the other hand, $\Delta\delta G_{solv}$ is always negative because the PCBAs in the right hand sides of Eqs. (5) and (6) have larger negative net-charge than those in the left hand sides, which results in greater stabilization due to the interaction with solvent water. ΔG, the sum of ΔE_{solute} and $\Delta\delta G_{solv}$, is positive in all the reactions. This means that the destabilizations of the solute electronic energy due to the reaction are partially compensated by the stabilization through solvation.

The second acid dissociation reactions show higher reaction free energies than the first for both PCBA and the PCBA-complex. ΔE_{solute} becomes higher from the first to the second acid dissociation reactions because of the charge localization in the product species. In contrast, $\Delta\delta G_{solv}$ becomes lower; that is, the divalent product species show greater stabilization by solvation. For the PCBA-complex, the magnitudes of both ΔE_{solute} and $\Delta\delta G_{solv}$ are smaller than those for PCBA, which is because the monosaccharide connected to the boric acid group allows delocalization of the excess charge and the solvent-accessible area near the boric acid group is smaller because of the steric bulk of the monosaccharide. The second acid dissociation reaction of the PCBA-complex has a stronger effect on the electronic structure of the molecule than solvent effects, which results in a 5 kcal mol^{-1} lower free energy change, ΔG, for the second acid dissociation reaction of the PCBA-complex than that of PCBA. Based on these results, we can say that the balance of the two effects determines the p*Ka* shift upon complex formation.

Table 3
Reaction free energies and their components. Units are in kcal mol^{-1}.

	ΔG	ΔE_{solute}	$\Delta\delta G_{solv}$	$\Delta\delta\mu_{KH}$	$\Delta\delta E_{dist}$
PCBA + $H_2O \rightarrow$ PCBA$^-$ + H_3O^+	28.74	175.04	−146.30	−156.55	10.25
PCBA$^-$ + $2H_2O \rightarrow$ PCBA^{2-} + H_3O^+	36.75	221.13	−184.37	−177.43	−6.94
PCBA-complex + $H_2O \rightarrow$ PCBA-complex$^-$ + H_3O^+	28.13	170.90	−142.77	−153.71	10.94
PCBA-complex$^-$ + $2H_2O \rightarrow$ PCBA-complex^{2-} + H_3O^+	31.22	199.42	−168.20	−165.58	−2.62

To gain more insight into the origins of the SFE changes, the solvation structures of the dissociation compounds were considered. In Fig. 3(a)–(d), the three-dimensional distribution functions (3D-DFs) of water around PCBA$^-$, PCBA^{2-}, PCBA-complex$^-$, and PCBA-complex^{2-}, respectively, are depicted. It is clear from these structures that the divalent species, namely PCBA^{2-} and PCBA-complex^{2-}, attract strongly with hydrogen atoms of the solvent water around the boric acid group through coulombic attraction. For a quantitative discussion, the radial distribution functions (RDFs) between the boric acid oxygen atom of PCBA and solvent water molecules are shown in Fig. 4. These RDFs were obtained by averaging 3D-DFs over the direction around the boric acid oxygen atom. In Fig. 4(a), a conspicuous peak of water hydrogen can be found at around $r = 2.0$ Å, whereas that of water oxygen appears at around $r = 3.5$ Å. The first peak of hydrogen for the PCBA divalent anion is more than twice as high as that for the PCBA monovalent anion. These features indicate that the hydrogen bond between solvent water and boric acid oxygen is enhanced by the second acid dissociation reaction of PCBA. In contrast, all the peaks of the PCBA-complex shown in Fig. 4(b) are lower than those of PCBA, which is due to the steric bulk of the monosaccharide. The hydrogen bond between solvent water and boric acid oxygen is also enhanced with the progression of the reaction of the PCBA-complex. The steric bulk of the monosaccharide means that the hydrogen bond is affected to a lesser extent than in the case of PCBA. For these reasons, $\Delta\delta G_{solv}$ has a higher value for the PCBA-complex than for PCBA.

Finally, let us consider the solubility of PCBA and the PCBA-complex. Fig. 5 shows the SFE of PCBA and the PCBA-complex plotted against pH. Here, the SFE related to the neutral species at pH x, $\Delta\delta G_{solv}(x)$, is defined as:

$$\Delta\delta G_{solv}(x) = \sum_i \alpha_i(x)\delta G_{solv,i} - \delta G_{solv,0} \qquad (i = 0, -1, -2), \tag{12}$$

where $\delta G_{solv,i}$ is the SFE of the species with net charge i. (Here we employed $\delta G_{solv,i}$ in pure water for all the pH range for simplicity, although the SFE actually changes depending on the solvent environment such as pH.) The SFE of PCBA has a plateau region (pH = 6.5–9). This can be explained from the bias of the equilibrium. As can be seen in Fig 1, the equilibrium of the acid dissociation reaction is biased to one-side, which indicates that PCBA takes a single specific dissociation state (PCBA$^-$) in the plateau region in addition to the lower (PCBA; pH < 3) and higher (PCBA^{2-}; pH > 12.5) regions. On the other hand, the PCBA-complex shows only a small shoulder at around pH = 5.5, because the PCBA-complex$^-$ cannot be a single component. (See Fig. 2.) The PCBA-

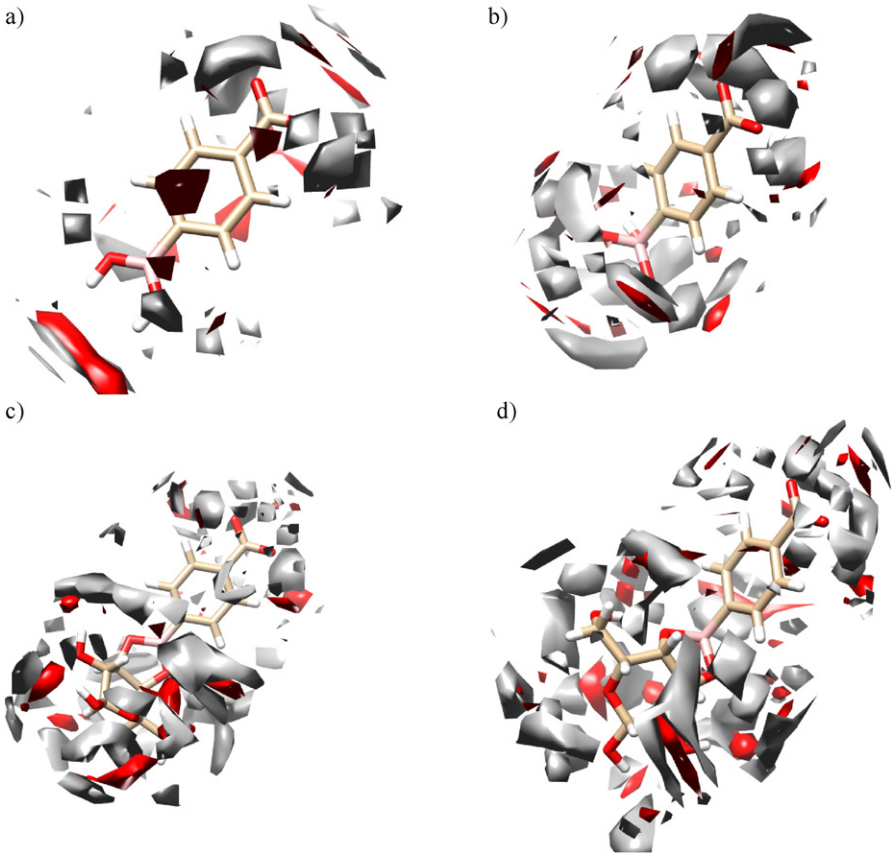

Fig. 3. 3D-DFs of solvent water around (a) PCBA$^-$, (b) PCBA^{2-}, (c) PCBA-complex$^-$, and (d) PCBA-complex^{2-}. Red and gray surfaces denote the 3D-DFs of water oxygen (isovalue = 3.0) and hydrogen (isovalue = 1.5), respectively.

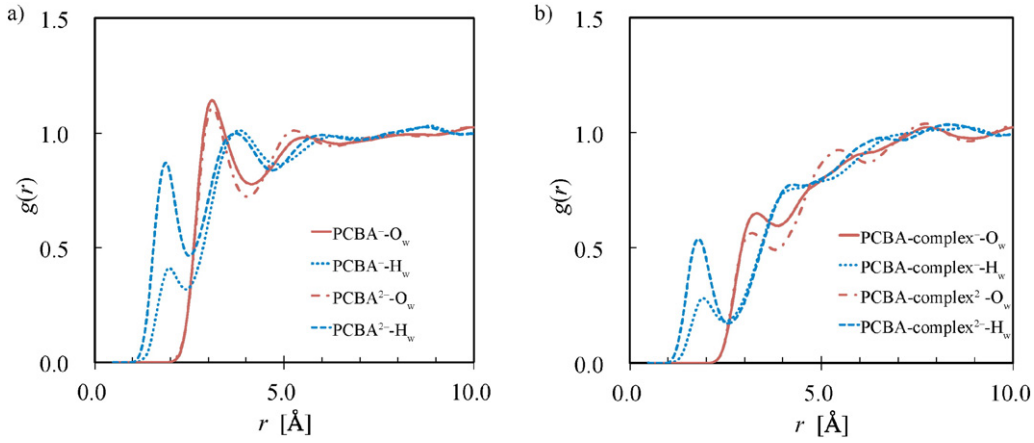

Fig. 4. RDFs of solvent water from specific center atoms of the solute molecule. Specific center atom: a) boric acid oxygen of PCBA and b) boric acid oxygen of PCBA-complex. The solid, dotted, dot-dashed, and dashed lines denote the water oxygen and water hydrogen around monovalent anion, and the water oxygen and water hydrogen around divalent anion, respectively.

complex shows greater stabilization under physiological conditions because the divalent anion form is dominant at this pH in the PCBA-complex, whereas the monovalent anion form is dominant in PCBA. This greater stabilization is thus the origin of the higher solubility of the PCBA-complex.

4. Conclusion

The effect of complex formation of PCBA with monosaccharide on the acid dissociation reaction has been investigated by applying the 3D-RISM-SCF theory. The acid dissociation reactions of PCBA and the PCBA-complex both involve two reaction steps. The first step is the dissociation of a proton from the carboxyl group, and the second step is the association of a hydroxide group to the boric acid moiety. The second p*K*a of the PCBA-complex showed a lower value than that of PCBA; that is, the PCBA-complex can take a more soluble form in the lower pH region.

The 3D-RISM-SCF analysis revealed at the molecular level the mechanism through which complex formation affects the solubility. Complex formation with the monosaccharide allows delocalization of the excess charge of the product species of the reaction, which means that the penalty on the solute electronic energy due to charge localization becomes lower in the PCBA-complex than in PCBA. Complex formation also changes the solvation structure. The boric acid group, which is the reaction center of the second acid dissociation reaction, is capped by the monosaccharide in the complex, which means that the solvent-accessible surface around the boric acid group is smaller than that in PCBA. This reduced area of accessible surface results in a smaller change of magnitude of the solvent effect upon reaction of the PCBA-complex. As a result of the balance between these two effects, the reaction free energy of the PCBA-complex is lower, leading to a lower p*K*a.

In the present study, we used a simple scheme to adjust overestimated computed p*K*a values. The corrected values worked well in our investigation; however, accurate p*K*a prediction is essential in the field of biochemistry and pharmacology, and an elaborated method beyond the simple empirical correction used herein is highly anticipated. Such studies, based on the 3D-RISM-SCF theory, are in progress.

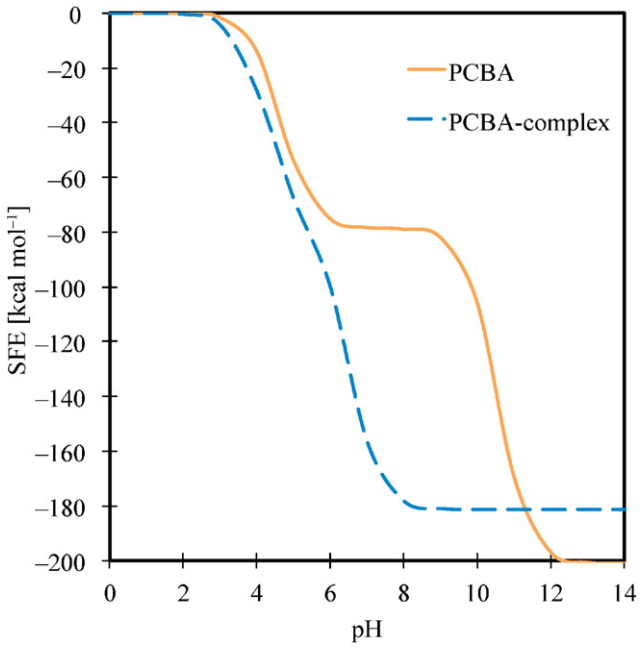

Fig. 5. SFE relative to the neutral species as a function of pH.

Acknowledgments

We are grateful to Ms. Yukako Kasai at Kyushu University, Dr. Toru Matsui at Tsukuba University, and Prof. Yasuteru Shigeta at Tsukuba University for their valuable comments on p*K*a evaluation. Numerical calculations were partly conducted at the Research Center for Computational Science, Institute for Molecular Science, National Institutes of Natural Sciences. We would like to thank the Next Generation Supercomputing Project, Nanoscience Program and the Strategic Programs for Innovative Research (SPIRE) and the Computational Materials Science Initiative (CMSI), Japan for their support. We are also grateful to Kyushu University Interdisciplinary Programs in Education and Projects in Research Development, and Grants-in-Aid (25410021, 26104526) from MEXT, Japan.

References

[1] Y. Kawabata, K. Wada, M. Nakatani, S. Yamada, S. Onoue, Int. J. Pharm. 420 (2011) 1.
[2] K. Thanki, R.P. Gangwal, A.T. Sangamwar, S. Jain, J. Control. Release 170 (2013) 15.
[3] H.D. Williams, N.L. Trevaskis, S.A. Charman, R.M. Shanker, W.N. Charman, C.W. Pouton, C.J. Porter, Pharmacol. Rev. 65 (2013) 315.
[4] S. Packer, J. Coderre, S. Saraf, R. Fairchild, J. Hansrote, H. Perry, Invest. Ophthalmol. Vis. Sci. 33 (1992) 395.
[5] J.A. Coderre, A.D. Chanana, D.D. Joel, E.H. Elowitz, P.L. Micca, M.M. Nawrocky, M. Chadha, J.O. Gebbers, M. Shady, N.S. Peress, D.N. Slatkin, Radiat. Res. 149 (1998) 163.
[6] A.H. Soloway, D.S. Gordon, J. Neuropathol. Exp. Neurol. 19 (1960) 415.
[7] K. Yoshino, A. Suzuki, Y. Mori, H. Kakihana, C. Honda, Y. Mishima, T. Kobayashi, K. Kanda, Strahlenther. Onkol. 165 (1989) 127.
[8] Y. Mori, A. Suzuki, K. Yoshino, H. Kakihana, Pigment Cell Res. 2 (1989) 273.
[9] T.M.B. Islam, K. Yoshino, A. Sasane, Anal. Sci. 19 (2003) 455.
[10] W.H. Sweet, A.H. Soloway, R.L. Wright, J. Pharmacol. Exp. Ther. 137 (1962) 263.

[11] A. Kovalenko, F. Hirata, J. Chem. Phys. 110 (1999) 10095.
[12] H. Sato, A. Kovalenko, F. Hirata, J. Chem. Phys. 112 (2000) 9463.
[13] J. Hong, N. Yoshida, S.-H. Chong, C. Lee, S. Ham, F. Hirata, J. Chem. Theory Comput. 8 (2012) 2239.
[14] N. Yoshida, Y. Kiyota, F. Hirata, J. Mol. Liq. 159 (2011) 83.
[15] S. Gusarov, T. Ziegler, A. Kovalenko, J. Phys. Chem. A 110 (2006) 6083.
[16] A. Kovalenko, F. Hirata, J. Mol. Liq. 90 (2001) 215.
[17] H. Sato, F. Hirata, J. Phys. Chem. A 102 (1998) 2603.
[18] H. Sato, F. Hirata, J. Phys. Chem. B 103 (1999) 6596.
[19] N. Yoshida, R. Ishizuka, H. Sato, F. Hirata, J. Phys. Chem. B 110 (2006) 8451.
[20] K. Kido, H. Sato, S. Sakaki, J. Phys. Chem. B 113 (2009) 10509.
[21] A.D. Becke, J. Chem. Phys. 98 (1993) 5648.
[22] J.D. Dill, J.A. Pople, J. Chem. Phys. 62 (1975) 2921.
[23] W.J. Hehre, R. Ditchfie, J.A. Pople, J. Chem. Phys. 56 (1972) 2257.
[24] A. Kovalenko, F. Hirata, J. Phys. Chem. B 103 (1999) 7942.
[25] A. Kovalenko, F. Hirata, Chem. Phys. Lett. 290 (1998) 237.
[26] J. Wang, W. Wang, P.A. Kollman, D.A. Case, J. Mol. Graph. Model. 25 (2006) 247.
[27] J. Wang, R.M. Wolf, J.W. Caldwell, P.A. Kollman, D.A. Case, J. Comput. Chem. 25 (2004) 1157.
[28] H.J.C. Berendsen, J.R. Grigera, T.P. Straatsma, J. Phys. Chem. 91 (1987) 6269.
[29] M.W. Schmidt, K.K. Baldridge, J.A. Boatz, S.T. Elbert, M.S. Gordon, J.H. Jensen, S. Koseki, N. Matsunaga, K.A. Nguyen, S. Su, T.L. Windus, M. Dupuis, J.A. Montgomery, J. Comput. Chem. 14 (1993) 1347.
[30] N. Yoshida, F. Hirata, J. Comput. Chem. 27 (2006) 453.
[31] J.M. Ho, M.L. Coote, Theor. Chem. Accounts 125 (2010) 3.
[32] T. Matsui, T. Baba, K. Kamiya, Y. Shigeta, Phys. Chem. Chem. Phys. 14 (2012) 4181.
[33] D.R. Lide (Ed.), CRC Handbook of Chemistry and Physics, 82 ed.CRC Press, New York, 2001.
[34] H.C. Brown, in: E.A. Braude, F.C. Nachod (Eds.), Determination of Organic Structures by Physical Methods, Academic Press, New York, USA, 1955.
[35] M.B. Smith (Ed.), March's Advanced Organic Chemistry: Reactions, Mechanisms, and Structure, 7 ed.Wiley, Hoboken, New Jersey, 2013.
[36] R.L. Pecsok (Ed.), Modern Methods of Chemical Analysis, 2 ed.John Wiley & Sons Inc., New York, 1976.